NANO LETTERS

Letter

pubs.acs.org/NanoLett

Buckled Silicene Formation on Ir(111)

Lei Meng,[†,§] Yeliang Wang,*[,†,§] Lizhi Zhang,[†,§] Shixuan Du,*[,†] Rongting Wu,[†] Linfei Li,[†] Yi Zhang,[†] Geng Li,[†] Haitao Zhou,[†] Werner A. Hofer,[‡] and Hong-Jun Gao*[,†]

[†]Institute of Physics, Chinese Academy of Sciences, Beijing 100190, China

[‡]Stephenson Institute for Renewable Energy, The University of Liverpool, Liverpool, L693BX, United Kingdom

ABSTRACT: Silicene, a two-dimensional (2D) honeycomb structure similar to graphene, has been successfully fabricated on an Ir(111) substrate. It is characterized as a $(\sqrt{7}\times\sqrt{7})$ superstructure with respect to the substrate lattice, as revealed by low energy electron diffraction and scanning tunneling microscopy. Such a superstructure coincides with the $(\sqrt{3}\times\sqrt{3})$ superlattice of silicene. First-principles calculations confirm that this is a $(\sqrt{3}\times\sqrt{3})$silicene/$(\sqrt{7}\times\sqrt{7})$Ir(111) configuration and that it has a buckled conformation. Importantly, the calculated electron localization function shows that the silicon adlayer on the Ir(111) substrate has 2D continuity. This work provides a method to fabricate high-quality silicene and an explanation for the formation of the buckled silicene sheet.

KEYWORDS: *Silicene, Ir(111), epitaxial growth, STM, LEED*

Silicene, wherein silicon atoms are substituted for carbon atoms in graphene, has recently created considerable interest among scientists, since such a new two-dimensional crystalline material, with a honeycomb structure similar to that of graphene,[1,2] is expected to have extremely useful physical properties.[3−11] Before silicene was conceived as a possible material, theorists and the experimental physicists had already analyzed in some detail very thin and narrow silicon nanostructures/nanowires.[12−17] Subsequently, theoretical models based on free-standing single-layer silicon and the conception of silicene were considered.[4] Also silicene strips have been studied experimentally.[18−22] Most recently, Cahangirov et al. conducted theoretical calculations and proposed that silicon atoms prefer to form a corrugated sheet structure.[5] In addition, a quantum spin Hall effect is predicted to be observable on silicene.[7]

Currently, the preparation of silicene in experiments is extremely difficult. As is widely known, graphene, a flat single layer of sp^2-bonded carbon atoms, can be exfoliated from graphite easily because of the weak interlayer interactions of graphite. However, silicene cannot be exfoliated from bulk silicon because silicon in the bulk is sp^3-hybridized. Breaking the covalent Si−Si bonds is too difficult to realize experimentally. Therefore, obtaining a 2D silicon sheet through exfoliation is impossible. Hence the primary method to fabricate silicene sheets is via epitaxial growth of silicon on solid surfaces. Only recently, the fabrication of such a sheet was reported on Ag(111) surface.[9,23−30] Apart from an Ag(111) substrate, silicene has been reported on zirconium diboride (ZrB_2) thin films grown on Si wafers.[10] The silicene on ZrB_2 is almost consistent with a structure referred to above.[25] Both studies observed a $(\sqrt{3}\times\sqrt{3})$ superstructure of silicene. These experimental findings are very interesting and attractive. However, only two kinds of substrates have been used in silicene growth so far. An in-depth analysis of controlled growth of silicene on other substrates, investigating its intrinsic physical properties in atomic detail, is thus still of great importance.

In the present work, we fabricated graphene-like silicon layer on an Ir(111) substrate. We deposited silicon on the Ir(111) surface and annealed the sample to 670 K, whereupon a distinct well-ordered structure appeared. Such structure was characterized as a $(\sqrt{7}\times\sqrt{7})$ superstructure with respect to the substrate by means of low energy electron diffraction (LEED) and scanning tunneling microscopy (STM). We then performed first-principles calculations based on density functional theory (DFT) and confirmed this superstructure as a $(\sqrt{3}\times\sqrt{3})$silicene/$(\sqrt{7}\times\sqrt{7})$Ir(111) configuration. Considering our experimental observations together with the calculated results allows the conclusion that silicene fabricated on this surface is a two-dimensional continuous layer with a buckled conformation.

Experiments were performed in an ultrahigh vacuum (UHV) system with a base pressure about 2×10^{-10} mbar. The Ir(111) substrate was cleaned by several cycles of sputtering and annealing until it yielded a distinct Ir(1×1) diffraction spot in a LEED pattern and clean surface terraces in STM images. Silicon was deposited on Ir(111) at room temperature under UHV conditions from a piece of silicon heated by a direct current. After deposition, the sample was annealed at 670 K for 30 min. To characterize its properties, we employed LEED to identify the superstructures macroscopically and STM to image the surface in atomic scale detail. Our DFT based first principles calculations were performed using the Vienna *ab*

Received: November 26, 2012
Revised: January 16, 2013
Published: January 18, 2013

   dx.doi.org/10.1021/nl304347w | *Nano Lett.* 2013, 13, 685−690

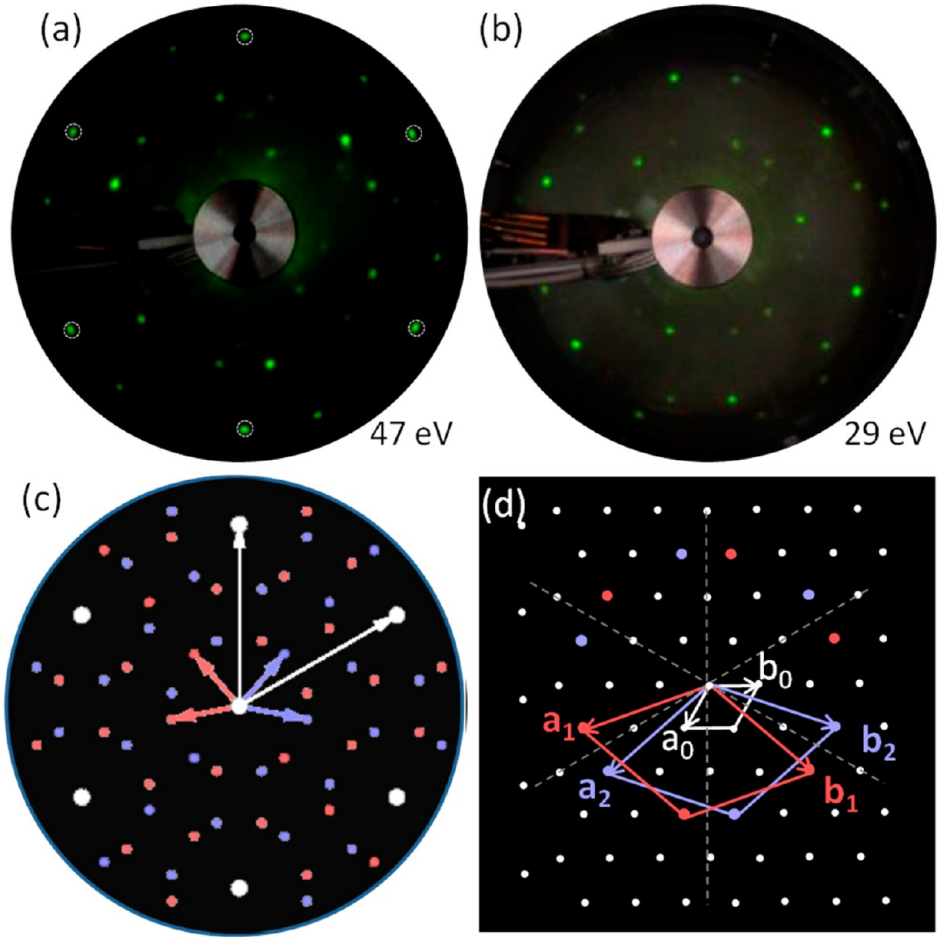

Figure 1. LEED patterns and the corresponding schematic diagrams of the silicon superstructure formed on the Ir(111) surface. (a) The outer six bright spots, highlighted by the dashed circles, originate from the 6-fold symmetry of the Ir(111) substrate. The additional diffraction spots are ascribed to the silicon adlayer. (b) LEED pattern obtained with lower incident electron beam energy. (c) Sketch of the diffraction spots shown in part a, where the reciprocal vectors of each group of spots are indicated by white, red, and blue arrows, respectively. (d) Schematic diagram of the diffraction spots in real space. These data reveal a $(\sqrt{7}\times\sqrt{7})$ superstructure of the silicon layer [lattice vectors (a_1, b_1) or (a_2, b_2)] with respect to the Ir(111) lattice [lattice vectors (a_0, b_0)]. Parts a and b were obtained at 47 eV and 29 eV, respectively.

initio simulation package (VASP).[31,32] The projector augmented wave (PAW) potentials were used to describe the core electrons, and the generalized gradient approximation of Perdew, Burke, and Ernzerhof (PBE) were used for exchange and correlation.[33] The periodic slab models include four layers of iridium, one layer of silicene, and a vacuum layer of 15 Å. All atoms were fully relaxed except for the bottom two substrate layers until the net force on every atom was less than 0.01 eV/Å. The energy cutoff of the plane-wave basis sets was 250 eV, and the *K*-points sampling was 9×9×1.

The structural characterization of the silicon layer formed on Ir(111) surface was first identified macroscopically by the arising LEED pattern, as shown in Figure 1a. The outer six bright spots, highlighted by the dashed circles, can easily be assigned to the Ir(111) substrate with 6-fold symmetry. The additional distinct diffraction spots then originate from the silicon superstructure. To detect this superstructure more clearly in this LEED pattern, we decreased the incident electron beam energy. This allows for a clearer imaging of the inner diffraction spots, as shown in Figure 1b. For clarity, we show a sketch map of the diffraction spots of the superstructure in reciprocal space (Figure 1c), where the reciprocal vectors of each group of spots are indicated by lines of different colors. Aside from the (1×1) diffraction spots of the Ir(111) lattice, two symmetrically equivalent domains exist, identified by red and purple spots, respectively. Aiming to understand these LEED patterns more thoroughly, a schematic diagram in real space consistent with the diffraction patterns is provided in Figure 1d. This diagram directly reveals the commensurability relation between the silicon adlayer and the substrate lattice. The silicon adlayer can easily be identified as a $(\sqrt{7}\times\sqrt{7})$ superstructure with respect to the Ir(111) substrate. The matrix of this $(\sqrt{7}\times\sqrt{7})$ superstructure is $\begin{bmatrix} 1 & -2 \\ 2 & 3 \end{bmatrix}$ or the equivalent $\begin{bmatrix} 2 & -1 \\ 1 & 3 \end{bmatrix}$, and the corresponding angles between the close-packed direction Ir[1−10] and the high symmetry direction of $(\sqrt{7}\times\sqrt{7})$ superstructure can be obtained simultaneously; they are 40.9° and 19.1°.

To characterize the silicon adlayer in real space, we subsequently used STM to investigate its geometric and electronic properties. The STM images in Figure 2a and b are obtained in different scanning areas on the same sample surface. The large scale STM image in Figure 2a shows a long-range order of the silicon superstructure. Comparing the directions between the superstructure in Figure 2a (indicated by a yellow arrow) and the one in Figure 2b (indicated by a blue arrow), it is noteworthy that they have different

dx.doi.org/10.1021/nl304347w | *Nano Lett.* 2013, 13, 685−690

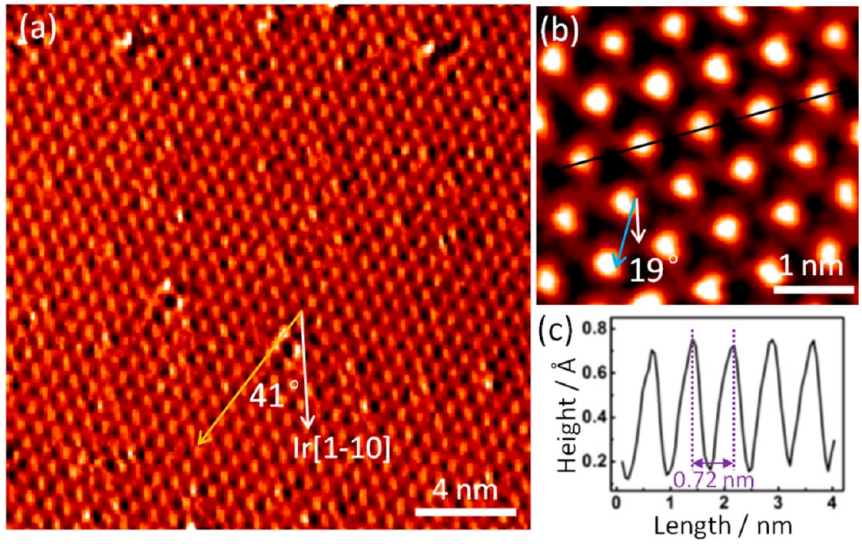

Figure 2. (a) STM topographic image (U = −1.45 V, and I = 0.25 nA), showing a $(\sqrt{7}\times\sqrt{7})$ superstructure of the silicon adlayer formed on the Ir(111) surface. The direction of this reconstruction is indicated by the yellow arrow. The close-packed direction of Ir[1−10] is indicated by the white arrow. The angle between the yellow and white arrows is around 41°. (b) STM image (U = −1.5 V, and I = 0.05 nA) of the silicon superstructure with another orientation, indicated by the blue arrow. The rotation angle between the blue and white arrows is about 19°. (c) Line profile along the black line in b, revealing the periodicity of the protrusions (0.72 nm) and a corrugation of around 0.6 Å for the silicon adlayer.

orientations with respect to the substrate Ir(111) lattice, with a relative rotation of 22°. This is consistent with the two equivalent domains detected in $(\sqrt{7}\times\sqrt{7})$ LEED patterns (see Figure 1). Figure 2c shows the line profile along the black line in Figure 2b, revealing that the periodicity of the bright protrusions in the STM image is about 0.72 nm. This distance is equal to the dimension of $(\sqrt{7}\times\sqrt{7})$ superlattice of Ir(111) (the lattice constant of Ir(111) is 0.271 nm, $\sqrt{7}\times 0.271$ nm = 0.72 nm). It is apparent that both, the orientations and the periodicity of the silicon superstructure detected by STM are in good agreement with the analysis of the LEED patterns, confirming that a $(\sqrt{7}\times\sqrt{7})$ silicon superstructure was formed on the Ir(111) surface. In addition, the profile reveals a corrugation of around 0.6 Å in the silicon adlayer. The corrugation implies that different silicon atoms in the adlayer have different apparent heights with respect to the underlying iridium surface, which will be analyzed by DFT calculations.

Apart from the brightest protrusions observed in Figure 2b, we note that there are two other regions showing different image contrast, marked by upward and downward triangles (Figure 3a), respectively. Obviously, the region inside the upward triangle is brighter than the one in the downward triangle. Considering the contrast differences in these regions, a honeycomb-like configuration of the silicon superstructure can be proposed and is depicted in Figure 3a: the darkest regions are the centers of the honeycomb lattice; the brightest protrusions are the vertexes (indicated by yellow dots) of the honeycomb. This honeycomb-like configuration is, in fact, a superlattice of the silicene structure. According to the prediction of previous theoretical studies,[3,5,7] the lattice constant of low-buckled free-standing silicene is about 3.8−3.9 Å. In that case, the lattice constant of the $(\sqrt{3}\times\sqrt{3})$ superlattice of the silicene is about 6.75 Å. This value is close to the periodicity of our observed structure (7.2 Å), the $(\sqrt{7}\times\sqrt{7})$ silicon superstructure on Ir(111). Thus, we propose the following model to account for our observations: a single layer silicon sheet is on top of the Ir(111) surface at a certain rotation angle. As the rotation angle between the close-packed direction of Ir[1−10] and the high symmetry direction of $(\sqrt{7}\times\sqrt{7})$ silicon superstructure is determined as 19.1° (Figure 2b) and the one between the lattice direction of (1×1) unit of silicene and its $(\sqrt{3}\times\sqrt{3})$ superlattice is 30°, we can deduce a rotation angle of 10.9° between the lattice direction of (1×1) unit of silicene and the substrate Ir[1−10]. In this model, the $(\sqrt{7}\times\sqrt{7})$ supercell of Ir(111) substrate nearly matches the $(\sqrt{3}\times\sqrt{3})$ superlattice of the silicon layer.

To prove our assumption and gain a deeper understanding of the silicene/Ir(111) system, we conducted DFT calculations and simulations of the STM observations using the Tersoff-Hamann approach.[34] During our calculations, several kinds of models (different locations of silicon atoms with respect to the substrate) were calculated. It turned out that the relaxed model in Figures 3c (top view) and 3d (perspective view) is the most stable configuration. The binding energy of this configuration is about 1.6 eV per silicon atom. The simulated STM image is shown in Figure 3b and the brightest protrusions in the formation of the hexagonal arrangement are indicated. In the simulations there is distinct contrast between the two triangular regions in a unit cell. These features are in excellent agreement with the STM observations in Figure 3a, verifying that the model of the $(\sqrt{3}\times\sqrt{3})$silicene/$(\sqrt{7}\times\sqrt{7})$Ir(111) configuration fundamentally resembles what we observed in experiments. The consistence between the STM simulation of the single silicon layer on Ir(111) and experimental STM image suggests that the silicon adlayer is a single layer. Figure 3c shows the top view of the relaxed lowest energy configuration. It reveals that there are six silicon atoms in one $(\sqrt{7}\times\sqrt{7})$ unit cell (the black rhombus): one silicon atom (the yellow one) is located directly on top of an iridium atom; two atoms are located at the hcp hollow and fcc hollow sites of the Ir(111) lattice as indicated in the rhombus; and the other three atoms are located at the bridge sites. These findings indicate that different silicon atoms are situated in different chemical environments with respect to the iridium surface, which are responsible for the buckled conformation of the silicon layer as analyzed below.

dx.doi.org/10.1021/nl304347w | Nano Lett. 2013, 13, 685−690

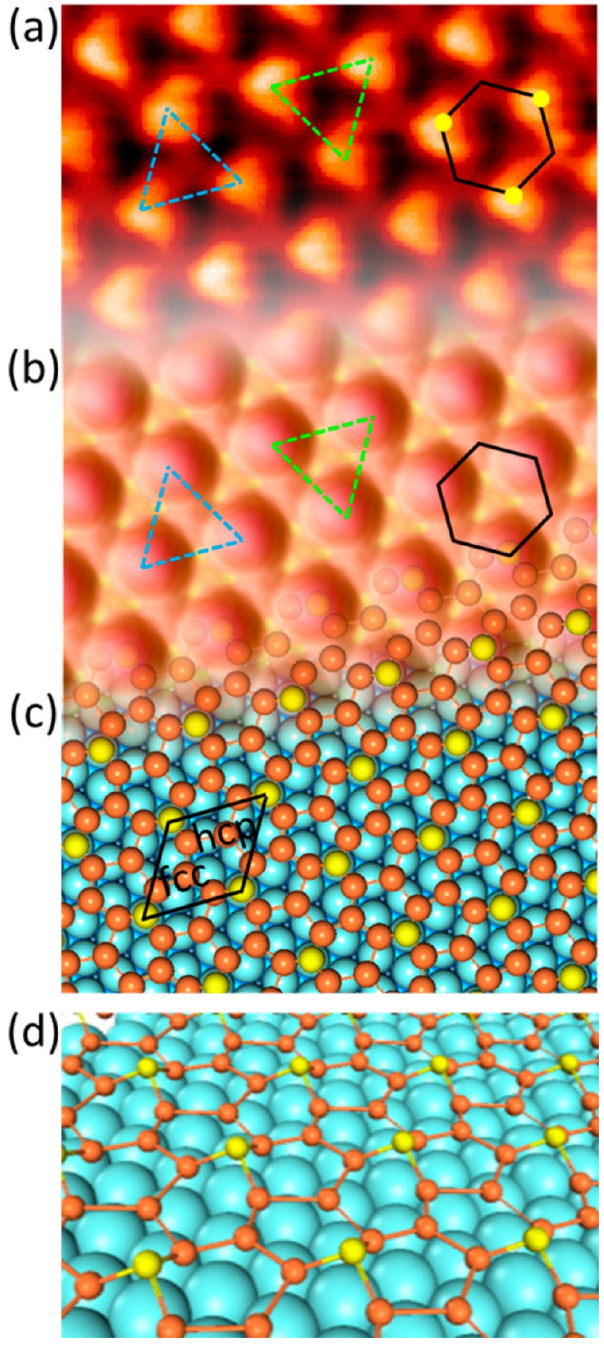

Figure 3. (a) Zoomed-in STM image of the silicon layer. Besides the brightest protrusions, two other regions showing different contrast are indicated by the upward and downward triangles. The honeycomb feature is indicated by the black hexagon. (b) Simulated STM image, showing features identical with the experimental results in the same triangles and hexagons. (c) Top view of the relaxed atomic model of the $(\sqrt{3}\times\sqrt{3})$silicene/$(\sqrt{7}\times\sqrt{7})$Ir(111) configuration. (d) Perspective view of the relaxed model in c, showing an undulated silicene on Ir(111) surface.

The relaxed model and the simulated STM image here provide a clear picture of the silicon arrangements in the adlayer corresponding to observations in the actual STM images. The silicon atoms at the top sites of the iridium lattice (the yellow balls in Figure 3b–d) correspond to the brightest protrusions (every other vertex of the honeycomb feature) exhibited in the STM image (Figure 3a). The less bright protrusion in the center of the upward triangle region (the other three vertexes) can be interpreted as the silicon atoms at fcc hollow sites, showing lower electron density of states compared with the silicon atoms on atop sites. The dim feature in the center of the downward triangular region is silicon atoms located at the hcp hollow sites with the lowest electron density of states. Figure 3d shows a perspective view of Figure 3c. It clearly exhibits the corrugation of the silicon adlayer on the Ir(111) surface. The silicon atoms are located at two different heights with respect to the substrate: the distance between the top silicon atoms (yellow balls) and the iridium substrate is about 2.83 Å; and the distance between the other silicon atoms (orange balls) and the substrate is around 2 Å. This height difference (0.83 Å) is to some degree consistent with the reported results of silicon sheets on Ag(111), where the height difference is 0.75 Å.[9] The undulation here clearly reveals a undulated silicon layer on Ir(111).

Although the silicon layer has a buckled structure with an undulation, implying an interaction between silicon layer and the substrate, we still infer that it is a continuous layer rather than an accumulation of fragments with several silicon atoms. To prove this argument, it needs to be established that interactions between silicon atoms in the sheet are much stronger than that of silicon atoms with the underlying substrate. To analyze these interactions, we have calculated the electron localization function (ELF),[35,36] which directly allows one to gauge chemical interactions from the charge localization between individual atoms. Figure 4a shows the top view of the overall ELF within the silicon layer with an ELF value of 0.6. Here, we see that chemical interactions exist between each pair of silicon atoms. This means the silicon atoms are well bonded to each other, showing a continuity of the silicene layer. To identify the bonding characteristics within each silicon pair clearly, the ELFs along the cross section of each silicon pair (annotated in Figure 4a) are displayed in Figure 4b–d. The value of the ELF is shown by the color scheme, where red represents the electrons that are highly localized and blue signifies electrons with almost no localization. It is clearly seen that electrons are localized to a large degree at the top-bridge and fcc-bridge silicon pair (the magnitudes of ELF values are in the range of 0.82, as shown in Figure 4b and c, respectively), identifying a covalent bonding between Si atoms. The hcp-bridge pair (Figure 4d) has slightly lower degree of electron localization in their intermediate location (ELF value is about 0.66). In conclusion, the ELFs presented here provide evidence for the covalent interaction existing between each silicon pair.

Considering now the interaction between the silicon layer and the underlying substrate, the extension of the silicene sheet on the substrate could be affected by the interplay between Si–Si interaction and Si–Ir interaction. For comparison, the ELF of the cross section between the silicon atom at the hcp site and its nearest iridium atom is shown in Figure 4e. The distance between such a silicon–iridium pair is the shortest one, and this is the position with the strongest interaction between the silicon layer and the substrate. However, the ELF value in this case is only 0.38, which is much smaller than those of any silicon pairs. ELF values of less than 0.5 correspond to an absence of pairing between electrons. Therefore, it can be concluded that the interaction is mainly of an electrostatic origin. This electrostatic interaction is not strong enough to affect the formation of Si–Si bonds and the extension of the silicon sheet. In short, the combined evidence as above-

dx.doi.org/10.1021/nl304347w | Nano Lett. 2013, 13, 685–690

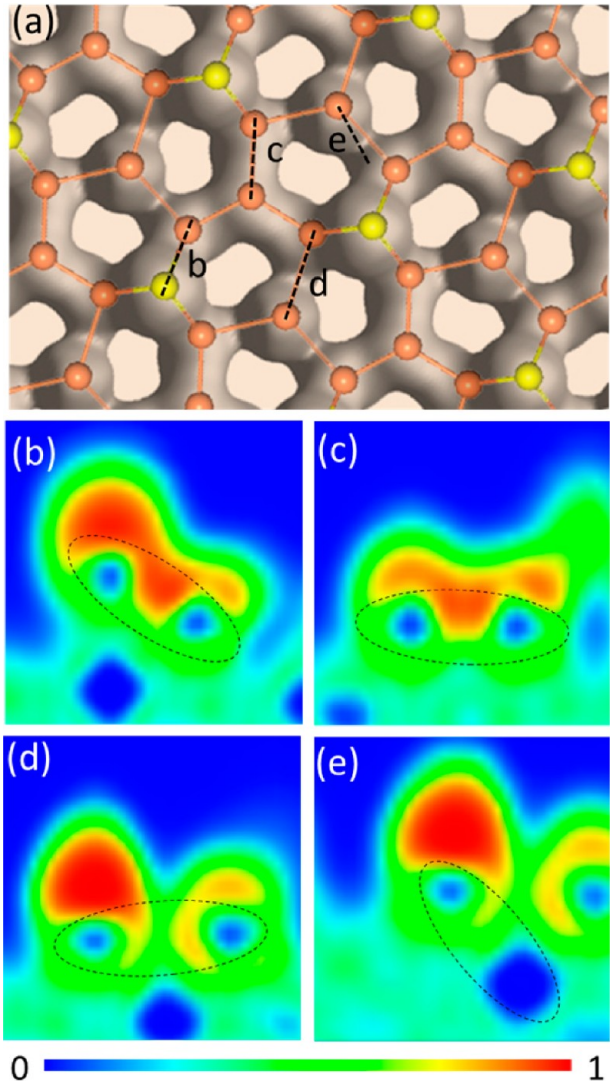

Figure 4. (a) Top view of the overall electron localization function (ELF) of the relaxed model with an ELF value of 0.6, demonstrating a continuity of the silicene layer. (b–d) The ELFs of the cross section between silicon pairs: (b) top-bridge pair; (c) fcc-bridge pair and (d) hcp-bridge pair, showing the covalent interaction existing between each pair of silicon atoms. The pairs are depicted by the dashed-line ellipses. (e) ELF of the cross section between the silicon atom at hcp hollow site and its nearest iridium atom. The ELF value here is at the range of green-blue region (about 0.38), indicating an electrostatic interaction. The color scale is shown at the bottom.

mentioned demonstrate that a two-dimensional continuous silicon layer—silicene—was indeed successfully fabricated on Ir(111).

In summary, we report the formation of silicene on Ir(111) and the corresponding geometric and electronic properties. The silicon adlayer shows a $(\sqrt{7}\times\sqrt{7})$ LEED pattern and has a honeycomb feature in STM images. This $(\sqrt{7}\times\sqrt{7})$ superstructure coincides with the $(\sqrt{3}\times\sqrt{3})$ superlattice of silicene, which is confirmed by DFT calculations. The location differences of the silicon atoms with respect to the substrate lattice are mainly responsible for the buckled conformation of the silicene sheet. By analyzing the electron localization function, covalent bonding is demonstrated to exist throughout the silicene layer. This work provides an effective method to produce high-quality silicene which allows us to investigate quantum phenomena of this novel two-dimensional material, and it may link up with potential applications in nanoelectronics and related areas.

AUTHOR INFORMATION

Corresponding Author

*E-mail: ylwang@iphy.ac.cn (Y.W.), sxdu@iphy.ac.cn (S.D.), or hjgao@iphy.ac.cn (H.J.G.).

Author Contributions

§These authors contributed equally to this work.

Notes

The authors declare no competing financial interest.

ACKNOWLEDGMENTS

The authors gratefully acknowledge financial support from MOST (Nos. 2011CB932700 and 2011CB921702), NSFC (Nos. 61222112 and 51210003), TRR61, SSC and CAS in China.

REFERENCES

(1) Geim, A. K.; Novoselov, K. S. *Nat. Mater.* **2007**, *6*, 183–191.
(2) Castro Neto, A. H.; Guinea, F.; Peres, N. M. R.; Novoselov, K. S.; Geim, A. K. *Rev. Mod. Phys.* **2009**, *81*, 109–162.
(3) Takeda, K.; Shiraishi, K. *Phys. Rev. B* **1994**, *50*, 14916–14922.
(4) Guzmán-Verri, G.; Lew Yan Voon, L. *Phys. Rev. B* **2007**, *76*, 075131.
(5) Cahangirov, S.; Topsakal, M.; Aktürk, E.; Şahin, H.; Ciraci, S. *Phys. Rev. Lett.* **2009**, *102*, 236804.
(6) Cheng, Y. C.; Zhu, Z. Y.; Schwingenschlögl, U. *Europhys. Lett.* **2011**, *95*, 17005.
(7) Liu, C.-C.; Feng, W.; Yao, Y. *Phys. Rev. Lett.* **2011**, *107*, 076802.
(8) Drummond, N.; Zólyomi, V.; Fal'ko, V. *Phys. Rev. B* **2012**, *85*, 075423.
(9) Vogt, P.; De Padova, P.; Quaresima, C.; Avila, J.; Frantzeskakis, E.; Asensio, M.; Resta, A.; Ealet, B.; Le Lay, G. *Phys. Rev. Lett.* **2012**, *108*, 155501.
(10) Fleurence, A.; Friedlein, R.; Ozaki, T.; Kawai, H.; Wang, Y.; Yamada-Takamura, Y. *Phys. Rev. Lett.* **2012**, *108*, 245501.
(11) Chen, L.; Liu, C.-C.; Feng, B.; He, X.; Cheng, P.; Ding, Z.; Meng, S.; Yao, Y.; Wu, K. *Phys. Rev. Lett.* **2012**, *109*, 056804.
(12) Singh, R.; Trenary, M.; Tanaka, T.; Sen, P.; Batra, I. *Phys. Rev. B* **2002**, *66*, 155416.
(13) Leandri, C.; Lay, G. L.; Aufray, B.; Girardeaux, C.; Avila, J.; Dávila, M. E.; Asensio, M. C.; Ottaviani, C.; Cricenti, A. *Surf. Sci.* **2005**, *574*, L9–L15.
(14) Rurali, R.; Lorente, N. *Phys. Rev. Lett.* **2005**, *94*, 026805.
(15) Léandri, C.; Oughaddou, H.; Aufray, B.; Gay, J. M.; Le Lay, G.; Ranguis, A.; Garreau, Y. *Surf. Sci.* **2007**, *601*, 262–267.
(16) De Padova, P.; Leandri, C.; Vizzini, S.; Quaresima, C.; Perfetti, P.; Olivieri, B.; Oughaddou, H.; Aufray, B.; Le Lay, G. *Nano Lett.* **2008**, *8*, 2299–2304.
(17) Vo, T. T. M.; Williamson, A. J.; Lordi, V.; Galli, G. *Nano Lett.* **2008**, *8*, 1111–1114.
(18) Kara, A.; Léandri, C.; Dávila, M. E.; Padova, P.; Ealet, B.; Oughaddou, H.; Aufray, B.; Lay, G. *J. Superconductor Novel Magn.* **2009**, *22*, 259–263.
(19) Le Lay, G.; Aufray, B.; Léandri, C.; Oughaddou, H.; Biberian, J. P.; De Padova, P.; Dávila, M. E.; Ealet, B.; Kara, A. *Appl. Surf. Sci.* **2009**, *256*, 524–529.
(20) Aufray, B.; Kara, A.; Vizzini, S. B.; Oughaddou, H.; Léandri, C.; Ealet, B.; Le Lay, G. *Appl. Phys. Lett.* **2010**, *96*, 183102.
(21) De Padova, P.; Quaresima, C.; Ottaviani, C.; Sheverdyaeva, P. M.; Moras, P.; Carbone, C.; Topwal, D.; Olivieri, B.; Kara, A.; Oughaddou, H.; Aufray, B.; Le Lay, G. *Appl. Phys. Lett.* **2010**, *96*, 261905.

(22) De Padova, P.; Kubo, O.; Olivieri, B.; Quaresima, C.; Nakayama, T.; Aono, M.; Le Lay, G. *Nano Lett.* **2012**, *12*, 5500−5503.
(23) Lin, C. L.; Arafune, R.; Kawahara, K.; Tsukahara, N.; Minamitani, E.; Kim, Y.; Takagi, N.; Kawai, M. *Appl. Phys. Exp.* **2012**, *5*, 045802.
(24) Jamgotchian, H.; Colignon, Y.; Hamzaoui, N.; Ealet, B.; Hoarau, J. Y.; Aufray, B.; Biberian, J. P. *J. Phys.: Condens. Matter* **2012**, *24*, 172001.
(25) Feng, B.; Ding, Z.; Meng, S.; Yao, Y.; He, X.; Cheng, P.; Chen, L.; Wu, K. *Nano Lett.* **2012**, *12*, 3507−11.
(26) Enriquez, H.; Vizzini, S.; Kara, A.; Lalmi, B.; Oughaddou, H. *J. Phys.: Condens. Matter* **2012**, *24*, 314211.
(27) Chiappe, D.; Grazianetti, C.; Tallarida, G.; Fanciulli, M.; Molle, A. *Adv. Mater.* **2012**, *24*, 5088−5093.
(28) Le Lay, G.; De Padova, P.; Resta, A.; Bruhn, T.; Vogt, P. *J. Phys. D: Appl. Phys.* **2012**, *45*, 392001.
(29) Kaltsas, D.; Tsetseris, L.; Dimoulas, A. *J. Phys.: Condens. Matter* **2012**, *24*, 442001.
(30) Arafune, R.; Lin, C.-L.; Kawahara, K.; Tsukahara, N.; Minamitani, E.; Kim, Y.; Takagi, N.; Kawai, M. *Surf. Sci.* **2013**, *608*, 297−300.
(31) Vanderbilt, D. *Phys. Rev. B* **1990**, *41*, 7892−7895.
(32) Kresse, G.; Furthmuller, J. *Phys. Rev. B* **1996**, *54*, 11169−11186.
(33) Perdew, J. P.; Burke, K.; Ernzerhof, M. *Phys. Rev. Lett.* **1996**, *77*, 3865−3868.
(34) Tersoff, J.; Hamann, D. R. *Phys. Rev. B* **1985**, *31*, 805−813.
(35) Becke, A. D.; Edgecombe, K. E. *J. Chem. Phys.* **1990**, *92*, 5397−5403.
(36) Savin, A.; Jepsen, O.; Flad, J.; Andersen, O. K.; Preuss, H.; Vonschnering, H. G. *Angew. Chem., Int. Ed. Engl.* **1992**, *31*, 187−188.